



## City Research Online

### City, University of London Institutional Repository

---

**Citation:** Lockett, R. D., Liverani, L., Thaker, D., Jeshani, M. & Tait, N. P. (2013). The characterisation of diesel nozzle flow using high speed imaging of elastic light scattering. *Fuel*, 106, pp. 605-616. doi: 10.1016/j.fuel.2012.10.065

This is the accepted version of the paper.

This version of the publication may differ from the final published version.

---

**Permanent repository link:** <https://openaccess.city.ac.uk/id/eprint/13540/>

**Link to published version:** <https://doi.org/10.1016/j.fuel.2012.10.065>

**Copyright:** City Research Online aims to make research outputs of City, University of London available to a wider audience. Copyright and Moral Rights remain with the author(s) and/or copyright holders. URLs from City Research Online may be freely distributed and linked to.

**Reuse:** Copies of full items can be used for personal research or study, educational, or not-for-profit purposes without prior permission or charge. Provided that the authors, title and full bibliographic details are credited, a hyperlink and/or URL is given for the original metadata page and the content is not changed in any way.

---

---

---

City Research Online:

<http://openaccess.city.ac.uk/>

[publications@city.ac.uk](mailto:publications@city.ac.uk)

---

# **The Characterisation of Diesel Nozzle Flow using High Speed Imaging of Elastic Light Scattering**

**\*R.D. Lockett, L. Liverani, D. Thaker, M. Jeshani, and <sup>1</sup>N.P. Tait**

**School of Engineering & Mathematical Sciences  
City University London  
Northampton Square, EC1V 0HB  
London, UK**

**<sup>1</sup> Shell Global Solutions (UK)  
Shell Technology Centre,  
Thornton, Chester, CH1 3SH, UK**

## **ABSTRACT**

Two identical, conventional six-hole, valve-covered orifice (VCO) diesel injectors have been modified in order to provide optical access to the region below the needle, and the nozzle-flow passages. This has been achieved through the removal of the metal tips, and their replacement with transparent acrylic tips of identical geometry.

These two identical injectors were employed in order to offer comparability between the measurements. One of them had a dark, anodised inner surface at the base, while the other had a silvered inner surface at the base. Elastic scattering of incident white light from the internal cavitating flow inside the nozzle holes of the optically accessible diesel injector tips was captured on a high-speed electronic camera. The optical image data was obtained for three injector rail pressures ranging from 200 bar to 400 bar, and for five diesel fuels of varying density, viscosity, and distillation profile, in order to identify variations in cavitation flow behaviour inside the nozzle hole passages.

A set of mean time-resolved diesel fuel flow images were obtained from thirty successive fuel injection pulses, for each operating condition, for each injector. The mean cavitation image occurring in the nozzle holes was converted to the mean proportion of nozzle hole area producing cavitation-induced optical scattering. The mean normalised area images were then

analysed, and were able to demonstrate the anticipated inverse relationship between injected fuel mass and cavitation volume fraction (indicated by mean normalised area), and the effect of fuel viscosity and distillation profile on cavitation volume fraction (again indicated by mean normalised area)

**Key Words:** diesel nozzle flow, cavitation, valve covered orifice, VCO diesel injector, elastic light scattering, imaging.

\* Corresponding Author

Email: r.d.lockett@city.ac.uk

Tel. (w) 44 (0)20 7040 8812

(m) 44 (0)7595 289996

## 1. INTRODUCTION

Modern common rail direct injection diesel engines operate through the injection of high pressure liquid diesel fuel directly into the engine cylinders. The fuel is normally injected through a number of nozzle holes located at the base of an injector. The fuel is subjected to large pressure gradients inside the injector and across the nozzles, which may cause local boiling of the fuel to create local pockets of fuel vapour. This type of flow is called cavitation flow, and is associated with unstable, unsteady vapour cavities forming inside the flowing fuel [1 – 3].

Chaves and others have previously identified the likelihood of cavitation occurring in the internal flow inside these injectors [1, 2, 4 – 7]. Internal cavitation flow occurring inside fuel injectors is believed to produce a number of effects on the internal fuel flow and the injector. Some of these are listed below:

- (1) Nozzle cavitation is believed to reduce the injected fuel mass in an unpredictable manner, which can result in an unpredictable fuel/air mixture formation in the engine. This may affect the combustion that develops, and/or engine out emissions [8 – 11].
- (2) Nozzle cavitation is believed to affect the atomisation of the fuel jets into droplets as the jets enter the engine cylinders [6, 7, 9 – 13].
- (3) Cavitation occurring near injector surfaces may cause surface erosion, and ultimately injector failure [14 – 16].

A significant amount of research work relevant to high pressure diesel fuel injection equipment (FIE) has been conducted in large scale model injectors offering excellent optical access through flow matching [6, 7, 17 – 21].

Two clearly distinguishable types of cavitation flow have been identified in large scale studies. These are geometric cavitation and string cavitation. Geometric cavitation is observed to form in the nozzle passages immediately following the nozzle inlet holes, and it is believed to be caused by the large drop in local pressure occurring in the fuel flow as it enters the nozzle holes. The local pressure gradient gives rise to conditions that facilitate local boiling. Geometric cavitation appears to be initiated as a dense foam of micro-bubbles developing in the liquid phase, which evolves into a connected volume of fuel vapour

extending from the hole inlet along the interior wall of the nozzle passage towards the hole exit [3, 22 – 24]. Alternatively, string cavitation is believed to form as a result of very intense flow vorticity, causing a low pressure region at the centre of the vortical flow [2, 3, 25, 26]. This may give rise to the conditions necessary for the formation of a string-like vapour cavity at the centre of the vortical flow. String cavitation has been observed as a highly transient phenomenon which occurs inside the nozzle sac. They appear as thin strings of fuel vapour, usually connecting the flow between adjacent holes.

Geometric cavitation and string cavitation have both been observed in optically accessible real-size injectors [27 – 29], providing justification for the flow studies in large scale model injectors.

It is interesting to note that a number of experiments have been conducted on biodiesel injection, atomisation and mixing in diesel engines [30 – 32]. The authors have reported that the spray characteristics of biodiesel are somewhat different to that of conventional diesel, and have suggested that the susceptibility of biodiesel to develop internal cavitation flow may be lower than conventional diesel fuel.

This paper reports the results of an experimental study of cavitation flow occurring inside the nozzles of modified, real-size, optically accessible VCO diesel injectors using white light scattering. The experiment aimed to identify whether different diesel fuels produced different amounts of cavitation flow, and whether it was possible to employ simple optical techniques to discriminate between the cavitation flows developed, and the physical variables responsible. A limited report has been published elsewhere [32].

## **2. EXPERIMENTAL ARRANGEMENTS**

### **2.1 The Optically Accessible Injectors**

Two identical VCO diesel injectors had their metal tips (including the nozzle holes) machined off and polished. One of these injector bodies was left unchanged, while the bottom surface of the other was anodised. The replacement optically accessible acrylic injector tips were manufactured by hand in the City University engineering workshop, copying the design of the VCO tip. A schematic of the arrangement is shown in Figure 1. It

is important to note that the acrylic tip attached to the injector below the needle seat, ensuring that the acrylic tip did not suffer any damage during needle opening and closure.

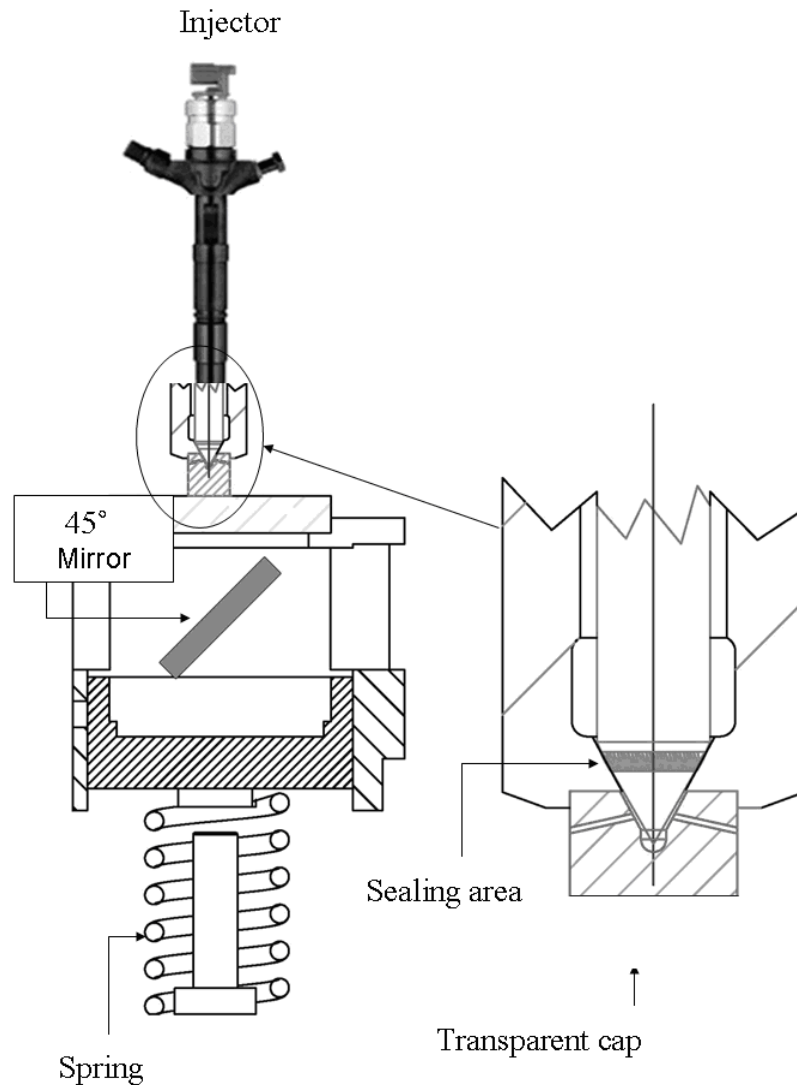


**Figure 1:** Mounting Configuration of the Optically Accessible VCO Injector

The injector was mounted at the top of a hollow cylindrical frame constructed from steel (as shown in Figure 1). The injector was fixed in a hole at the top end of the cylindrical frame. The acrylic tip was held in place with a transparent acrylic disc of approximately 10 mm thickness and 40 mm diameter. The acrylic disc was mounted on a pre-loaded sprung steel ring with an open centre. The adjustable compression force exerted on the tip by the disk ensured that the tip could withstand up to 600 bar rail fuel pressure without leaking.

The diesel fuel was injected through the nozzle holes in the injector tip into atmospheric air in the laboratory. Consequently, an air extraction facility was placed adjacent to the injector in order to protect personnel from exposure to atomised diesel fuel in the laboratory space.

## **2.2 The Fuel Injection System**

A variable speed motor was employed to drive a Denso diesel common rail pump. A laptop computer was employed to control a prototype programmable electronic control unit, which in turn, controlled the fuel pressure in the common rail. The diesel fuel temperature could be controlled by passing the diesel fuel through a heat exchanger sited between the fuel tank and the high pressure pump, although this facility was bypassed in these experiments.

The modified injector was connected to a prototype Denso-Toyota high pressure diesel common rail injection system. The prototype electronic fuel injection system enabled user control of the common rail pressure and the injection timing and duration. The injection parameters were controlled from a personal computer equipped with National Instruments data control cards, which controlled the electronic injector driver. The electronic injector driver sent a high voltage square wave pulse to a magnetic solenoid, located in the injector. The switching of the magnetic solenoid activated the injector needle, allowing high pressure fuel to pass through the injector. The mean time-resolved needle lift for this type of injector was measured using an inductive sensor, and is shown on the timing diagram presented in Figure 2.

The needle lift appeared to be gradual with an approximately constant lift rate of 0.118 mm/ms for approximately 4 ms, followed by a short period of approximately 0.3 ms in the neighbourhood of maximum lift, followed by an approximately constant rate of needle return for a period of approximately 1.6 ms. The needle reached its final seal position at approximately 6 ms after the electronic start-of-injection signal. This lift profile was due to the relatively low common rail pressure of 200 bar to 400 bar, and is typical for engines operating at idle, or low/part load, when the common rail pressure remains relatively low (400 bar - 600 bar).

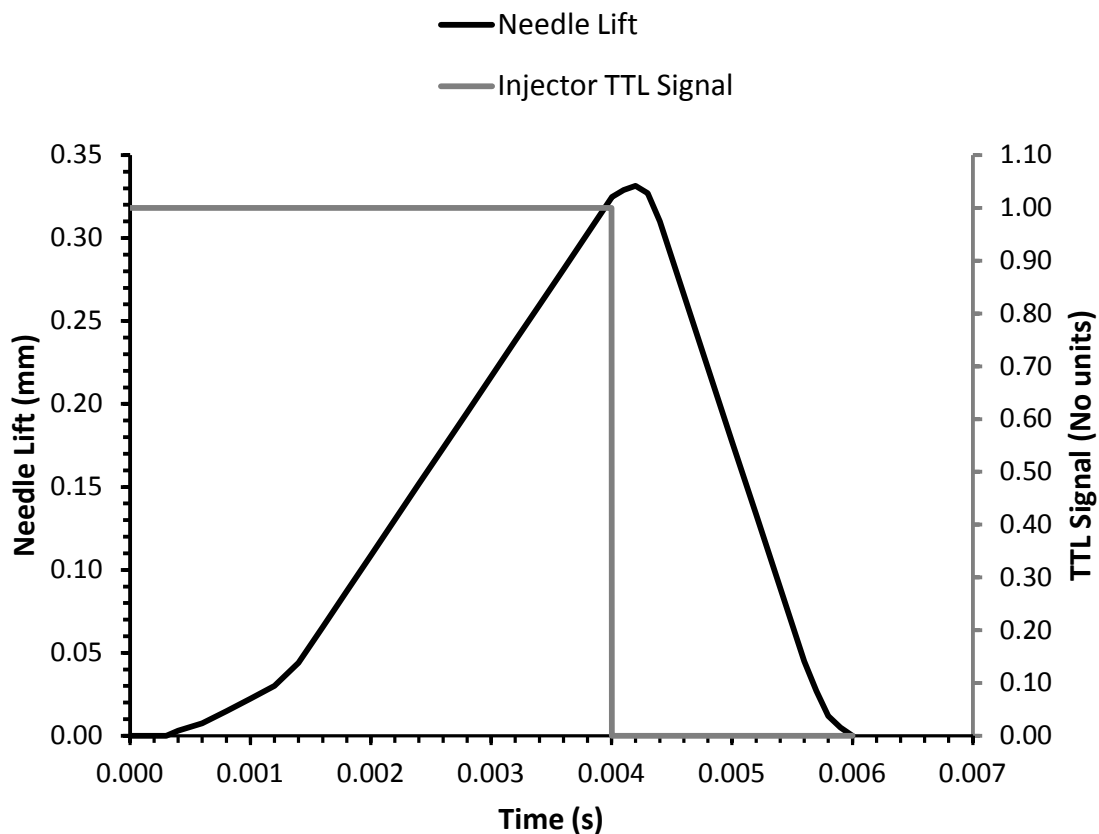


**Figure 2:** Graph of Needle Lift and Injection Pulse plotted against Time.

The injectors employed in this study were designed for maximum rail pressures of approximately 1200 bar to 1400 bar. During high load operation, the high fuel pressure normally facilitates the development of a large needle lift rate. The needle normally reaches its highest point within 0.5 ms, and remains open at its highest position until the magnetic circuit is turned off.

### 2.3 Diesel Fuel Properties

Five different diesel fuel samples were tested. Table 1 shows the main physical properties of the five samples. Four different properties were investigated amongst the five fuel samples provided. The first property to be investigated was the fuel density. Fuel sample B had a density that was 2.5 % larger than fuel sample A, while the other dominant properties (viscosity and distillation profile) were very similar. The second property to be investigated was kinematic viscosity, together with distillation profile. The kinematic viscosity of fuel

sample C was 95% larger than that of fuel sample B, and the distillation profile of sample C produced a mean temperature shift of approximately + 40 °C relative to fuel sample B for each distilled 10% interval. The third property to be investigated was the effect of adding a fatty acid methyl ester (FAME) to the base diesel. Fuel sample D comprised an 80:20 mixture (v/v) of fuel A and FAME, effectively making a B20 diesel. The fourth property to be investigated was the effect of adding a proprietary additive to fuel A, which then became fuel sample E.

**Table 1 - Physical Properties of Tested Diesel Fuel Samples**

<b>Diesel Fuel Type</b>	<b>A</b>	<b>B</b>	<b>C</b>	<b>D</b>	<b>E</b>
<b>Density @ 15 °C (g/cm<sup>3</sup>)</b>	0.823	0.840	0.840	0.834	0.823
<b>Kinematic Viscosity @ 40 °C (cSt)</b>	2.218	2.11	4.107	2.564	2.218 (est.)
<b>Additional Detail</b>				B20 (20% FAME)	Proprietary additive

## **2.4 The Optical Arrangement**

The optical arrangement is shown in Figure 3. Continuous white light obtained from a collimated Arri Pocket Par 400 W lamp was passed through a 150 mm diameter glass lens with 25 cm focal length. The focussed light was reflected up through the hollow metal tube using a 45 deg mirror. The light was further focussed onto the acrylic tip, by passing it through an infra-red filter and a 40 mm diameter lens with 50 mm focal length, followed by a beam splitter plate arranged at 45 deg.

Back-scattered light obtained from the cavitating diesel in the nozzle passages was reflected onto a high speed Photron Ultima APX–RS video camera using a Nikon 50 mm f1.2 camera lens, reverse coupled to 60 mm lens extension tubes. This arrangement facilitated high resolution imaging of approximately 10 μm/pixel. The Photron APX–RS camera was

configured to obtain 512 pixel x 512 pixel 10-bit monochrome images at 10 kHz. The use of this camera in this manner facilitated real-time capture of individual injection events.

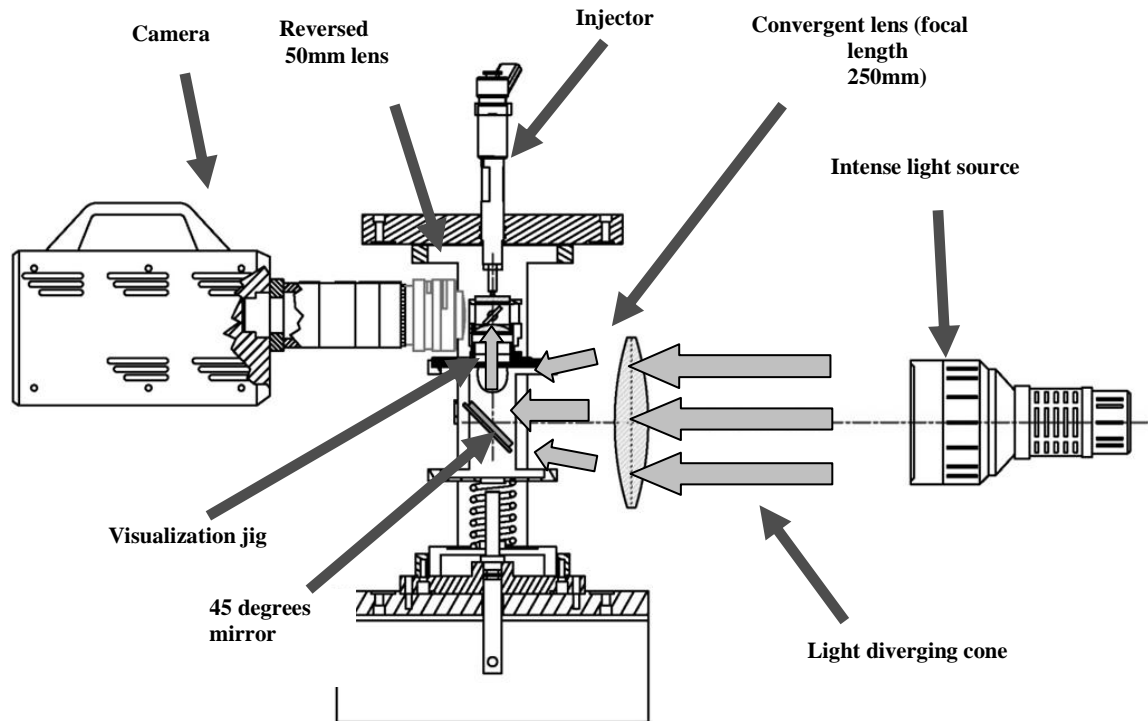


**Figure 3:** Schematic of Optical Arrangement

The camera was configured to begin capturing images synchronous with the leading edge of the electronic pulse sent to the injector. On receipt of the injector pulse, the camera took 100 frames at 10 kHz frame rate for 10 ms duration. Each frame was subjected to an exposure duration of 1.0  $\mu$ s. In order to protect the camera and the camera lens from exposure to atomised diesel oil, absorbent paper was placed inside a toroidal receiver, which was placed around the injection region.

### 3. EXPERIMENTAL METHODOLOGY

The main objective of the experiment was to determine whether diesel fuel samples of differing density, viscosity and boiling profile produced identifiably different cavitation flow inside the nozzle holes. If differences could be identified, a second objective would be to discover whether the differences could be employed to discover relevant trends or

dependencies. In this regard, five diesel fuel samples were employed in this study. The diesel fuel properties are presented in Table 1.

Modern high pressure common rail diesel injection systems operate at pressures of between 1000 bar and 2000 bar at high load. Due to the properties of acrylic, the maximum operating rail pressure that could be achieved during this study was 400 bar. Operating at lower pressure therefore required longer injection duration in order to inject a comparable quantity of diesel.

It was considered desirable to examine the internal flow during needle lift and return, and steady-state maximum lift. Consequently a fixed fuel injection pulse of 4 ms was employed for all tests. The needle lift and the injector pulse are shown in Figure 2.

### **3.1 Hydrodynamic Erosion of Acrylic Nozzles**

It was observed that the acrylic injector tips experienced significant hydro-erosion when subjected to multiple injections at 400 bar rail pressure. The ongoing erosion of the acrylic surface at the inner entrance to the nozzle holes caused the cavitation flow inside the nozzle passages to change over time. These changes were assessed over time by subjecting a small number of test injector tips to approximately 1000 injections each at 400 bar rail pressure. The dataset obtained from the 1000 injections were grouped into 10 subsets of 100 injections each. The mean, normalised scattering area as a function of time relative to the injection was obtained for each subset of 100 injections, resulting in 10 chronologically obtained datasets for each tip. The cavitation graphs were then compared with each other in order to determine the rate of deterioration of the acrylic nozzle tips.

It was discovered that the nozzle tips produced consistent cavitation scattering for approximately 300 injections at 400 bar. A more conservative limit of 200 injections per tip was imposed for all of the fuel tests at all pressures in order to ensure consistency and repeatability of the flow inside the acrylic nozzle tips.

### 3.2 Nozzle Repeatability

As the many identical acrylic injector tips were manufactured individually in-house, it was considered necessary to develop and apply a manufacturing quality control test. This was done in order to ensure that small manufacturing variations in the nozzle tips did not cause a significant effect on the diesel cavitation. Three newly manufactured tips were tested using diesel sample A at 300 bar and 400 bar rail pressure respectively. The optical scattering from the cavitation flow obtained from the three tips was compared using the image processing methodology discussed below. The resulting graphs of normalised cavitation scattering area obtained as a function of time for the three nozzles is shown in Figure 4.

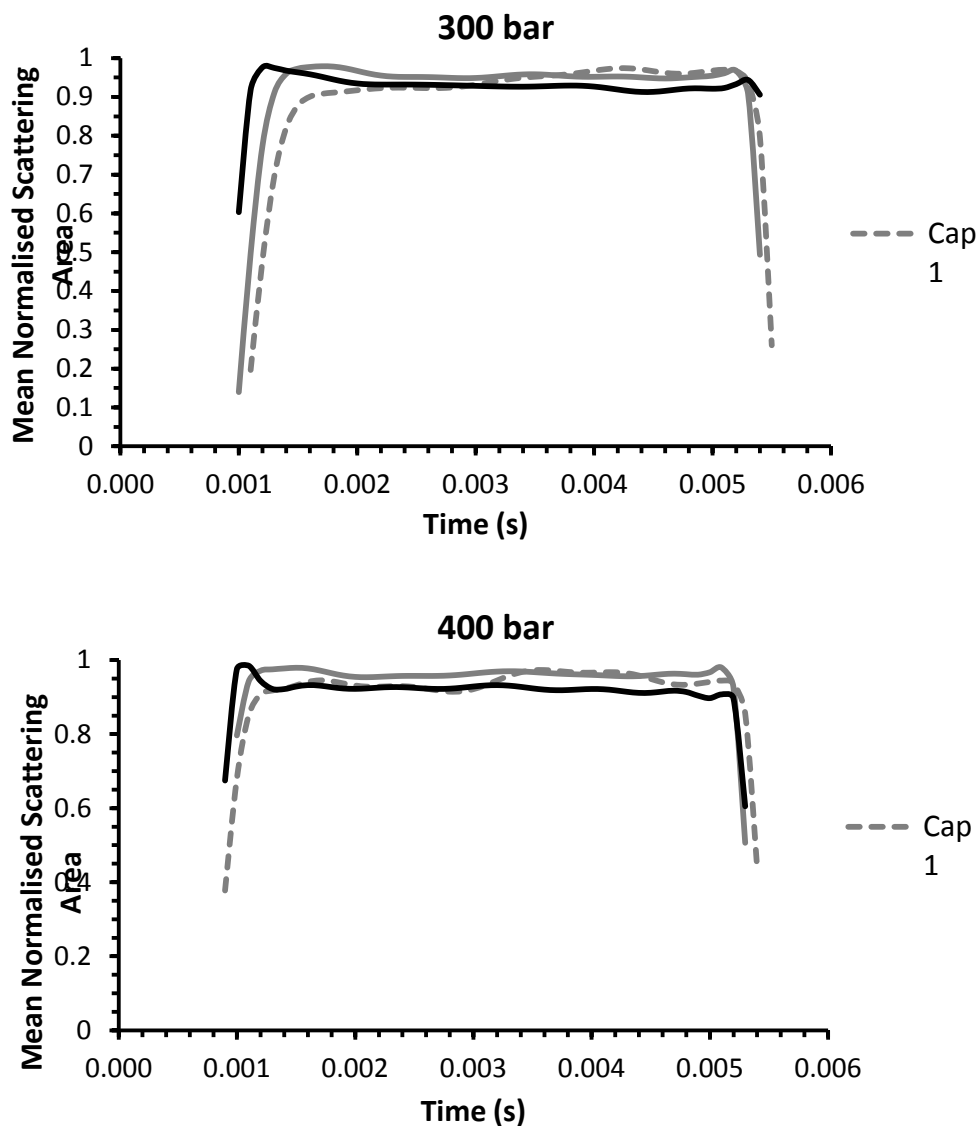


**Figure 4: Comparison of the Relative Mean Normalised Scattering Area as a Function of Injection Time for Three Identical Injector Tips at 300 bar and 400 bar Rail Pressure (Anodised Injector).**

The first graph in Figure 4 shows the normalised cavitation scattering area as a function of time obtained at 300 bar rail pressure, while the second graph shows the normalised cavitation scattering area as a function of time at 400 bar rail pressure. The six curves taken together in the two graphs show that the three optically accessible acrylic tips produce very similar internal cavitation scattering, with an overall variation of approximately 1.5 % from the mean. This sets a quantitative minimum criterion of 3% variation for discrimination between different diesel fuel samples and optical tips. However, this rule does not apply to multiple sets of measurements employing the same optical tip.

### **3.3 Experimental Test Procedure**

An experimental session combining one of the two injector bodies, and a new injector tip, together with a specified fuel consisted of: (1) obtaining 40 background images of the injector body and tip containing 100 % liquid fuel, followed by (2) obtaining 30 sets of 100 images synchronous with 30 injections at 200 bar, 300 bar and 400 bar respectively.

Following each experimental session, the mean injected fuel mass was measured for each diesel fuel sample. This was achieved by changing the optical accessible injector to an identical conventional injector, followed by injecting the diesel fuel sample through the conventional injector for 1000 injections into a sealed receiving vessel. The number of injections was electronically counted. The mean injected fuel mass was determined by dividing the net mass of fuel injected by the total number of injections. The results of these measurements are presented in Table 2.

The diesel fuel required changing following an experimental session. The fuel system was drained, and then refilled with the new diesel fuel sample. This fuel sample was passed through the system, and then drained. This was defined as one flush. The fuel system was flushed in this manner four times, before the new fuel was used for the next experimental session. This flushing process ensured that less than 1 % of the original diesel fuel remained in the system from session to session.

#### 4. IMAGE PROCESSING

Each experimental session involved the injection of one of the diesel fuel samples into laboratory air, using three common rail pressures of 200 bar, 300 bar and 400 bar respectively. The camera was configured to capture 100 images of the internal cavitation flow at 0.10 ms intervals for 10 ms duration, for each injection. Image data was obtained from 30 successive injections, making a total of 3000 images per fuel sample, per rail pressure, per injector.

Each set of 3000 images were numbered frame 1 to frame 3000. Frames 1, 101, 201, 301, 401 ... 2901 made up a subset of 30 images of the optical scattering from the diesel fuel inside the injector passages obtained at 0.1 ms after the leading edge of the start-of-injection (ASOI) electronic pulse. Frames 2, 102, 202, 302, 402 ... 2902 made up a subset of 30 images obtained at 0.2 ms after the leading edge of the SOI pulse, and so on to the subset of images defined by frame 100, 200, 300 ... 3000.

In order to express the processing of the data images mathematically, the pixel intensity on the raw data images was represented by  $S_{ij}^{klmp}$ , where  $S_{ij}^{klmp}$  represented the intensity of the pixel located on the CCD chip at the position defined by the row index  $i$  and the column index  $j$ ,  $i, j \in \{1,2,3,\dots,512\}$ . The index number  $k$  represents the frame number within a set of 100 time-resolved images for a single injection event, ranging from frame 1 to frame 100; while the index number  $l$  refers to the specific injection event, ranging from injection 1 to injection 30. The index number  $m$  refers to the diesel fuel sample tested, and ranges from 1 to 5, representing fuel samples A to E, the index number  $n$  refers to the three pressures tested, and ranges from 1 to 3, representing 200 bar, 300 bar and 400 bar respectively, while the index number  $p$  refers to the injector employed in the test, and ranges from 1 to 2.

For each fuel sample and each rail pressure, a set of 100 mean time-resolved cavitation images were determined by finding the mean images associated with frames 1, 101, 201, 301 ... 2901, frames 2, 102, 202, 302, ... 2902, frames 3, 103, 203, 303, ... 2903, and so on up to frames 100, 200, 300, ... 3000. This is expressed mathematically by

$$\overline{S_{ij}^{kmnp}} = \frac{1}{30} \sum_{l=1}^{30} S_{ij}^{klmnp} \quad (1).$$

Standard deviation images were also computed from the above data. These are expressed by

$$X_{ij}^{kmnp} = \sqrt{\frac{1}{29} \sum_{l=1}^{29} (S_{ij}^{klmnp} - \overline{S_{ij}^{kmnp}})^2} \quad (2).$$

40 background images were obtained for each experimental session. These pixel intensity data are represented by the indexed intensity variable  $B_{ij}^{mpq}$ , where the index numbers  $i, j, m$  and  $p$  retain their meaning from above, while the index number  $q$  refers to background image 1 to 40. A mean background image was calculated for each experimental session. This is expressed by

$$\overline{B_{ij}^{mp}} = \frac{1}{40} \sum_{p=1}^{40} B_{ij}^{mpq} \quad (3).$$

Processed data images were generated by subtracting the mean background images from the mean time-resolved cavitation images. These are expressed by

$$\overline{I_{ij}^{kmnp}} = \overline{S_{ij}^{kmnp}} - \overline{B_{ij}^{mp}} \quad (4).$$

An example of this form of image processing is shown in Figure 5. In order to process the captured optical data properly from the raw data image (the image on the left of Figure 5), the background image must be subtracted (the middle image). The processed image on the right is the final image obtained after background subtraction.

The scattering of light from the cavitating diesel fuel in the nozzles attached to the two injector bodies appeared different. The injector body with the anodised base (injector 1) had a background which was dark (as can be seen in Figure 5). White light striking cavitating surfaces in the cavitating flow was scattered in all directions, a proportion of which was captured by the 50mm f1.2 lens.

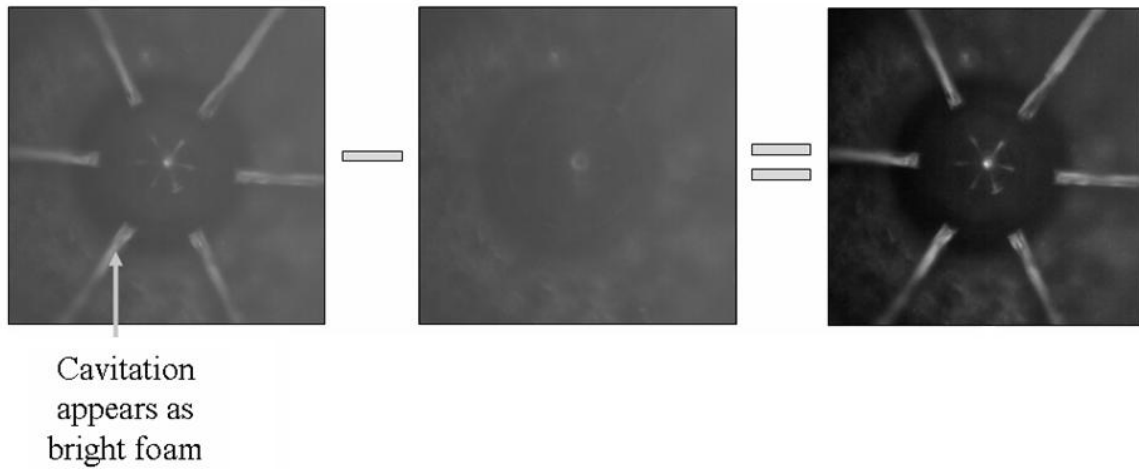


**Figure 5: Images showing Image Processing Methodology in Anodized Injector 1.**

The right hand image in Figure 5 is an image of the mean cavitation scattering obtained from the cavitation flow occurring in the nozzle passages of the optically accessible injector tip after background subtraction. The optical scattering captured on the video camera was being back-scattered from the cavitating diesel fuel, and appears as the six large bright streaks pointing away from the centre of the image.

The second injector (injector 2) with a silvered surface on the base of the injector body produced a bright background, scattering back the incident white light with high efficiency. White light incident on cavitating surfaces within the flow scattered incident white light away from the silvered surface, resulting in reduced white light scattered back towards the beam splitter and 50 mm lens. The resulting images appeared to show optical absorption. This effect is shown in Figure 6, which is a single-shot image obtained during cavitation flow occurring in the nozzle holes during a diesel fuel injection. When the mean background image was subtracted from the mean data images, the cavitating flow regions of interest showing optical absorption produced processed images that contained negative intensities. These negative intensities were converted to positive values by multiplying the entire set of processed images by -1.

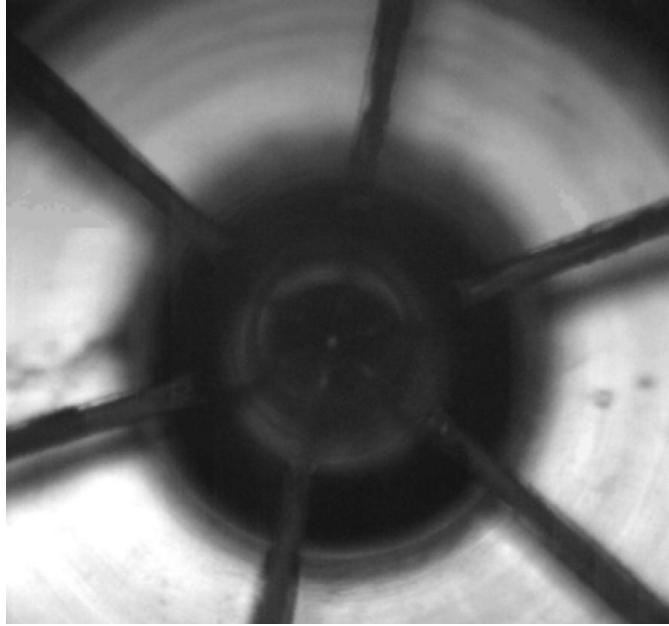


**Figure 6: Single-shot Image of Cavitating Flow Obtained from Silvered Injector 2.**

The images shown in Figures 5 and 6 suggest that very little optical distortion to the back-scattered rays of light travelling from the cavitating surfaces in the nozzle flow, through the acrylic tip and base, towards the beam-splitter, and into the 50 mm lens, occurs. This is because (1) the rays of light leaving the acrylic base that were imaged on the camera did so at nearly right angles to the acrylic disk surface, and (2) the refractive index of the diesel fuel samples and the acrylic nozzle tips and base were approximately 1.46 and 1.49 respectively [33]. This meant that the high speed video images of the optical scattering obtained from the cavitating flow surfaces contained very little refractive distortion.

The mean image frame intensity data defined by  $\overline{I_{ij}^{kmn}}$  were subjected to a threshold test as to whether cavitation was present or absent. This consisted of: (1) Creating a binary optical mask in software defined by the boundaries of the nozzle passages and centre. The mean processed data images were then multiplied by the binary mask image, resulting in scattered light intensity arising from cavitation flow occurring in the nozzle passages only; (2) Setting pixel values to zero where the actual intensity was smaller than 5 % of the mean intensity of scattered light obtained from the nozzle holes. Mathematically, this is expressed by determining the image mean scattering intensity obtained from the holes

$$\overline{I^{kmnp}} = \frac{1}{NM} \sum_{i=1}^N \sum_{j=1}^M \overline{I_{ij}^{kmnp}}, \quad (5)$$

where the values of  $i$ ,  $j$ ,  $N$  and  $M$  are limited to the pixels contained within the nozzle holes. The cavitation threshold test is then applied, expressed by the conditional

$$\text{If } \overline{I_{ij}^{kmnp}} < \frac{\overline{I^{kmnp}}}{20}, \text{ then set } \overline{I_{ij}^{kmnp}} = 0, \text{ else set } \overline{I_{ij}^{kmnp}} = 1. \quad (6)$$

The time-resolved binarised mean images were then converted to normalised area images. This was done by adding up the binary data within the nozzle passages. The total value obtained from the sum is the number of pixels producing significant optical scattering from the cavitation flow occurring in the nozzle holes. Dividing this value by the total number of pixels associated with the images of the nozzle passages provides the area fraction giving rise to significant optical scattering from cavitating surfaces inside the nozzles.

## 5. RESULTS AND DISCUSSION

### 5.1 Diesel Flow Measurements

Table 2 shows the total injected fuel mass for 1000 discrete injections of 4 ms TTL pulse duration at 400 bar rail pressure for all five fuels, together with the mean mass flow rate, the mean volume flow rate, the theoretical Bernoulli nozzle flow velocity  $v_B = \sqrt{2(p_{rail} - p_{back})/\rho_{diesel}}$ , the actual mean nozzle flow velocity,  $v_N = \dot{m}_{diesel}/\rho_{diesel}A_{nozzle}$ , the resultant mean discharge coefficient, and the mean Reynolds Number associated with each flow. The terms  $p_{rail}$ ,  $p_{back}$ ,  $\rho_{diesel}$ ,  $\dot{m}_{diesel}$ , and  $A_{nozzle}$  in the above expressions are the common rail pressure, the back pressure, the fuel density, the deduced mean mass flow rate of diesel in the injector nozzles, and the cross-sectional area of the injector nozzles respectively. The mean values for the mass flow rate, the volume flow rate, nozzle flow velocity, discharge coefficient and Reynolds Number were determined using a mean flow duration of 5 ms, obtained from the needle lift profile in Figure 2, and the cavitation flow profiles observable in Figures 7 to 11.

**Table 2 - Flow Parameters for Tested Diesel Fuel Samples**

<b>Diesel Fuel Type</b>	<b>A</b>	<b>B</b>	<b>C</b>	<b>D</b>	<b>E</b>
<b>Injected Fuel Mass (1000 injections)(g)</b>	52.63	52.56	53.13	55.40	54.63
<b>Mean Mass Flow Rate (g/sec)</b>	10.526	10.512	10.626	11.080	10.926
<b>Mean Volume Flow Rate (cm<sup>3</sup>/s)</b>	12.796	12.510	12.647	13.284	13.282
<b>Bernoulli Velocity (m/s)</b>	311.5	308.2	308.2	309.3	311.5
<b>Mean Nozzle Velocity (m/s)</b>	138.5	135.4	136.9	143.8	143.8
<b>Mean Discharge Coefficient</b>	0.4448	0.4395	0.4443	0.4650	0.4617
<b>Mean Nozzle Reynolds Number</b>	8745	8987	4668	7853	9077

A comparison of the properties associated with fuel samples A and B shown in Table 1, and the measured and deduced flow characteristics shown in Table 2 reveals that the larger density of fuel B relative to fuel A has resulted in a correspondingly reduced mean volume flow rate, nozzle velocity, and discharge coefficient.

A comparison of the properties associated with fuel samples B and C shown in Table 1 and 2 reveals that the 95 % larger kinematic viscosity in fuel sample C relative to fuel B (together with the heavier distillation profile), has resulted in a slightly larger mean mass flow rate, volume flow rate, nozzle flow velocity, and mean discharge coefficient.

Finally, bio-diesel sample D and fuel E have significantly larger mass flow rates, volume flow rates, mean nozzle flow velocities, and mean discharge coefficients than samples A, B and C. This is a consequence of the addition of 25 % FAME to fuel sample A to make sample D, and the proprietary additive added to sample A to make sample E.

## 5.2 Cavitation Flow Pressure Dependence

Figures 7 through to 11 show graphs of the mean normalised scattering area as a function of time during the injection for both anodised and silvered injectors, for all five fuel samples, and for the three rail pressures tested (200 bar, 300 bar and 400 bar). A new tip was employed for each of the fuel samples, but the same tip was employed for the three rail pressures tested.

The mean normalised scattering area was observed to increase consistently as a function of rail pressure throughout the injection process for fuel samples A, B, C, and D for both anodised and silvered injectors. On the other hand, fuel E produced normalised cavitation scattering area profiles at 200 bar and 300 bar that was larger than for the 400 bar profile at the beginning of the fuel injection. However, the 400 bar normalised cavitation scattering area profiles increased for time  $t > 2$  ms, achieving a mean value greater than that for both the 200 bar and the 300 bar data until the end of the injection. This was consistent with the pressure dependent normalised scattering area profiles obtained from the other fuel samples.

These observations require an assessment in the context of the nozzle flow cavitation number, which is defined to be  $Ca = p_{rail} - p_{back} / p_{back} - p_v$ , where  $p_v$  is the local saturated vapour pressure of the liquid, and the other variables retain their meaning from the previous section. The cavitation number identifies the relative propensity of a liquid to cavitate as a result of local variations in hydrodynamic stress. The nozzle flow cavitation numbers associated with the diesel nozzle flows presented in Figures 7 to 11 were approximately 197 at 200 bar rail pressure, 296 at 300 bar rail pressure, and 394 at 400 bar rail pressure. The increase in cavitation number with the increasing common rail pressure was accompanied by a monotonically increasing normalised cavitation scattering area for all of the fuel samples (as expected).

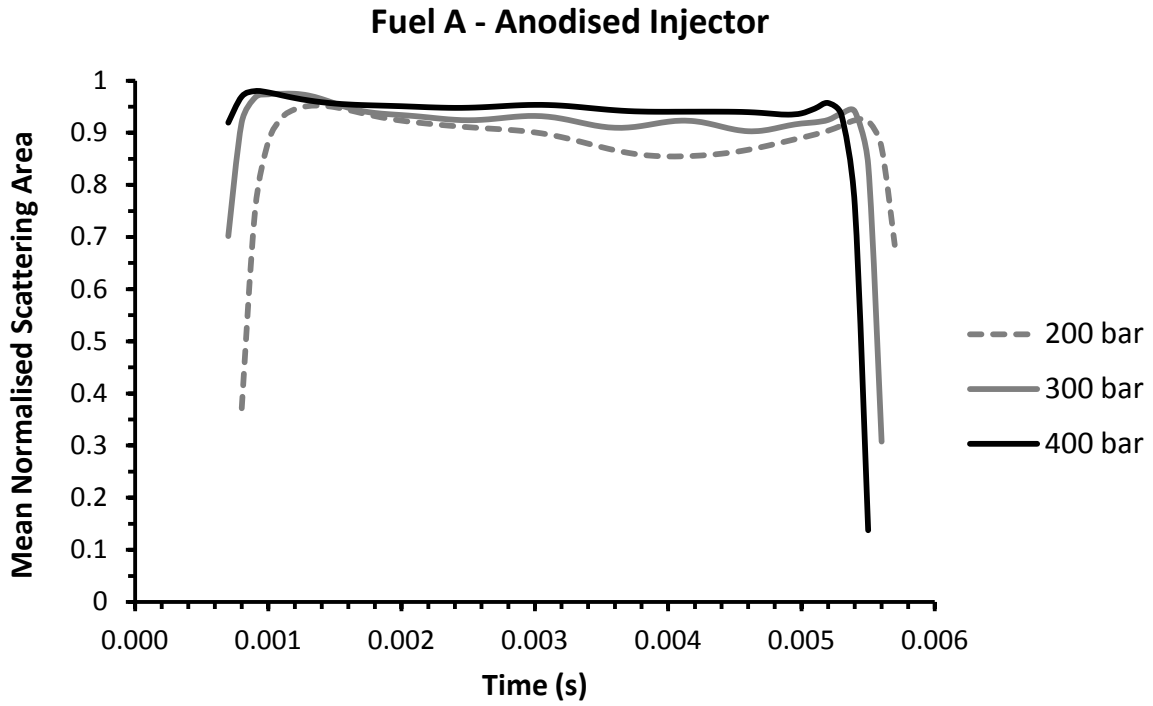


**Figure 7 (a): Graph of Normalised Cavitation Scattering Area for Fuel A as a Function of Time During the Injection for the Anodised Injector**

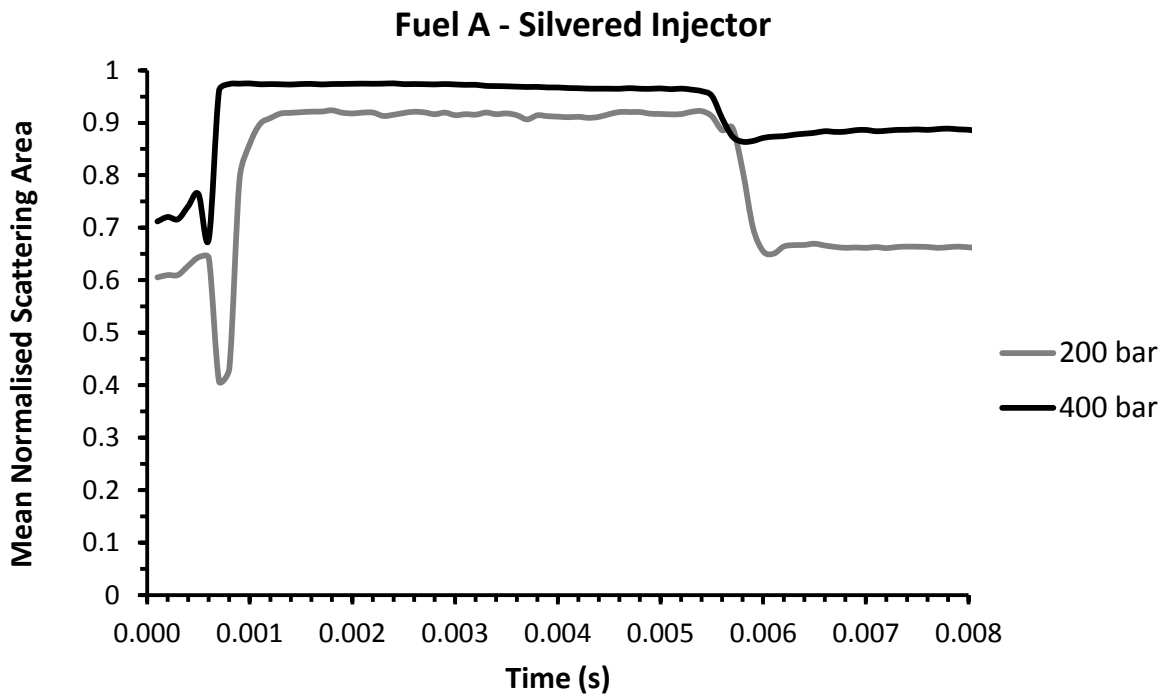


**Figure 7 (b): Graph of Normalised Cavitation Scattering Area for Fuel A as a Function of Time during the Injection for the Silvered Injector**

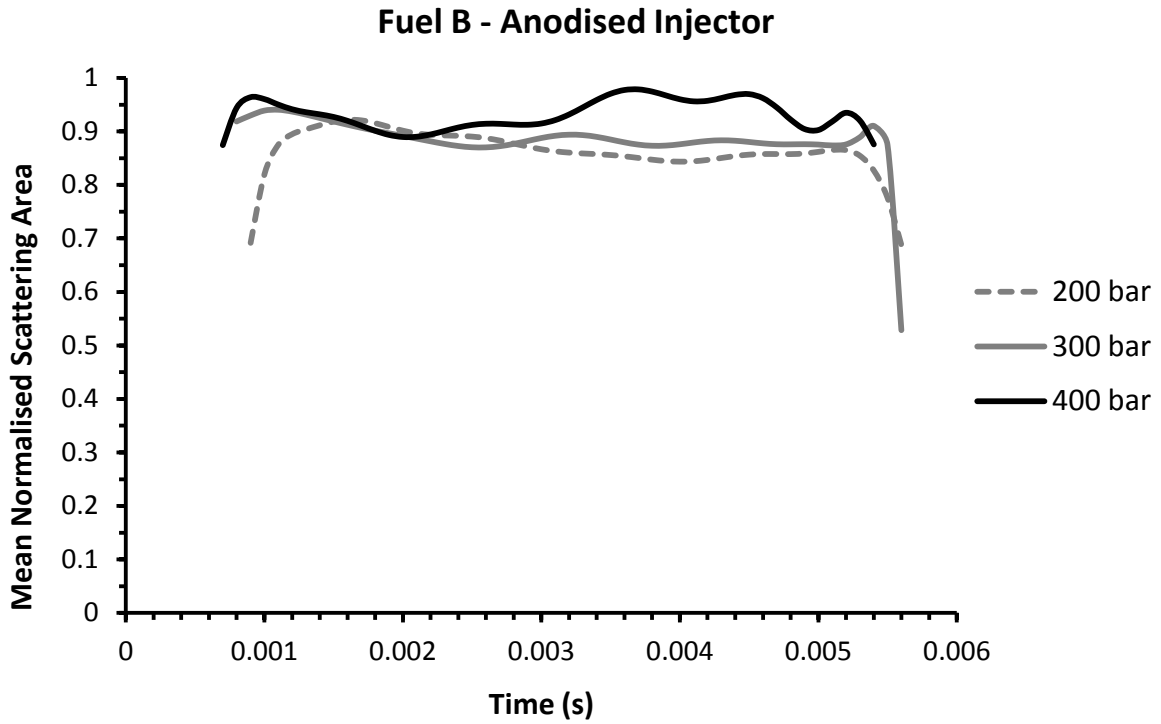


**Figure 8 (a): Graph of Normalised Cavitation Scattering Area for Fuel B as a Function of Time during the Injection for the Anodised Injector**

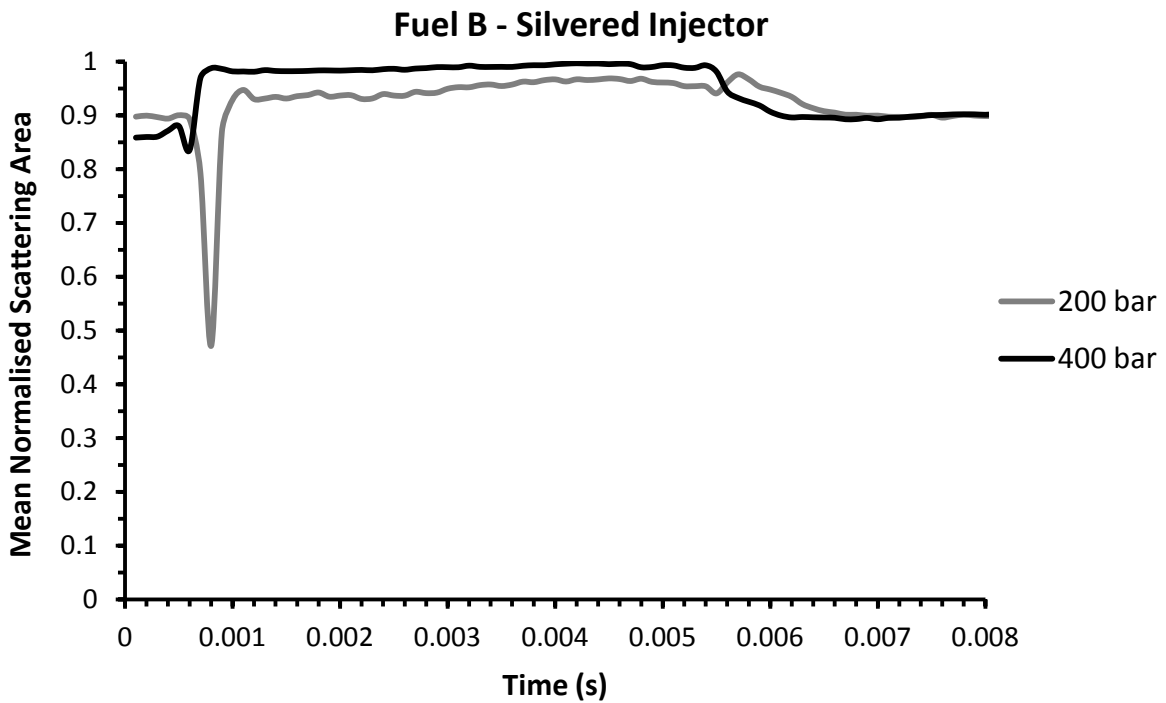


**Figure 8 (b): Graph of Normalised Cavitation Scattering Area for Fuel B as a Function of Time during the Injection for the Silvered Injector**

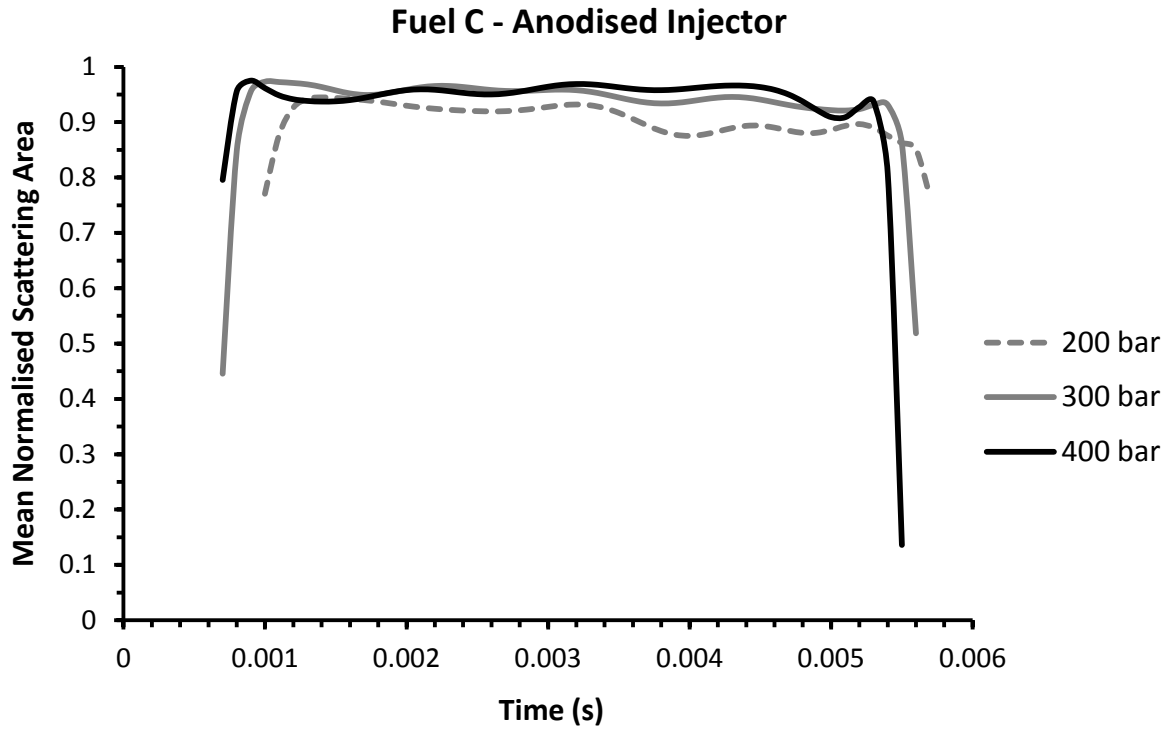


**Figure 9 (a): Graph of Normalised Cavitation Scattering Area for Fuel C as a Function of Time during the Injection for the Anodised Injector**

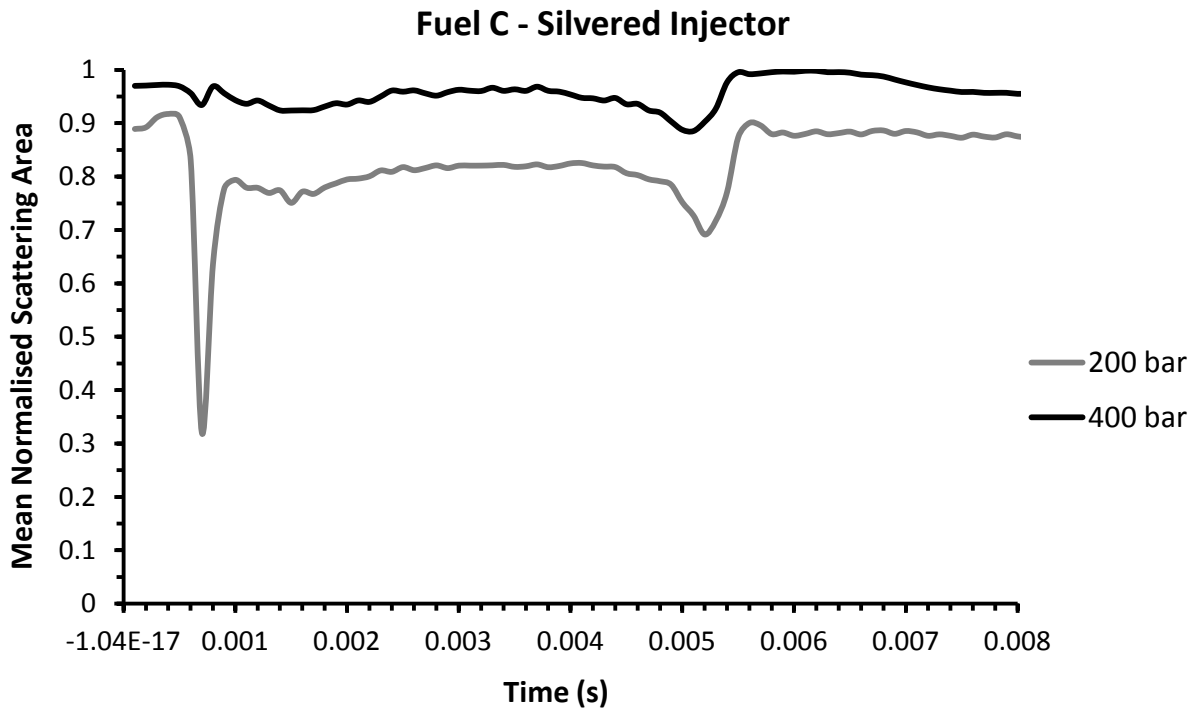


**Figure 9 (b): Graph of Normalised Cavitation Scattering Area for Fuel C as a Function of Time during the Injection for the Silvered Injector**

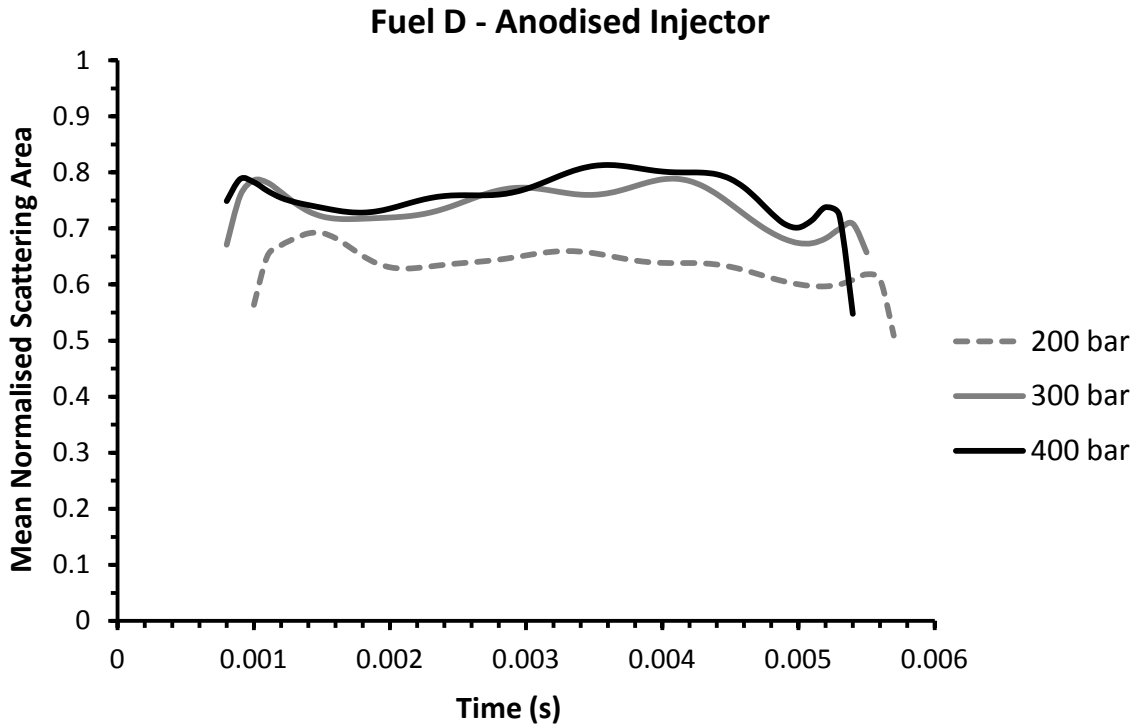


**Figure 10 (a): Graph of Normalised Cavitation Scattering Area for Fuel D as a Function of Time during the Injection for the Anodised Injector**

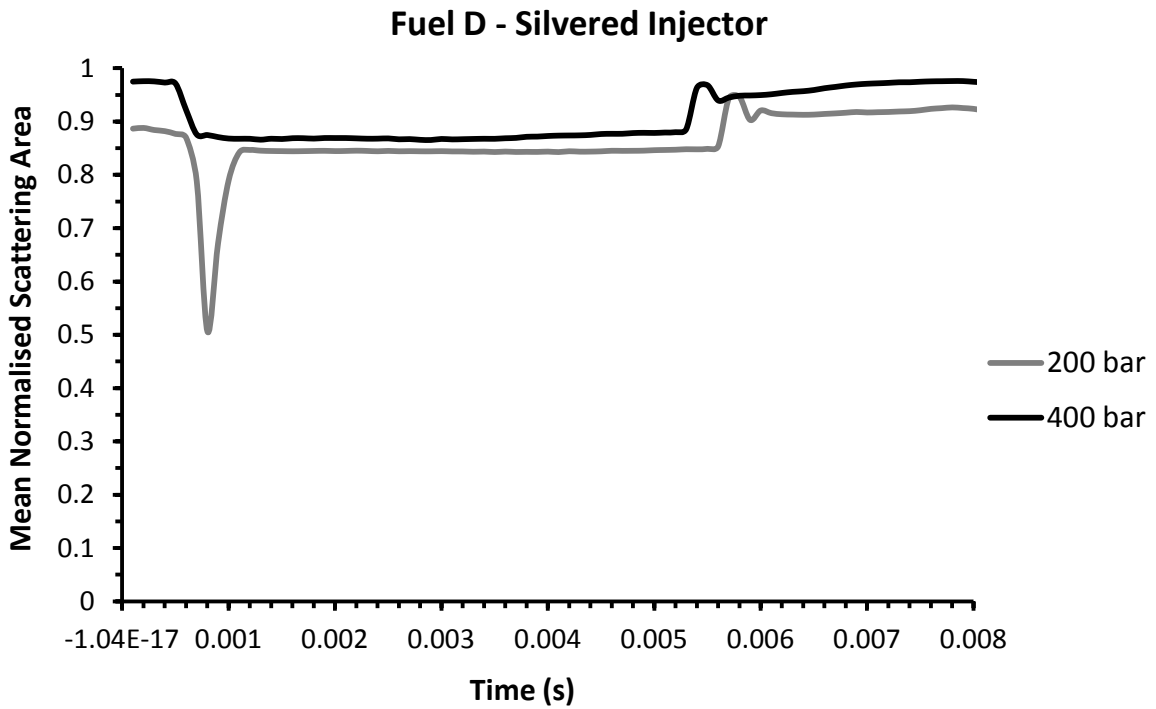


**Figure 10 (b): Graph of Normalised Cavitation Scattering Area for Fuel D as a Function of Time during the Injection for the Silvered Injector**

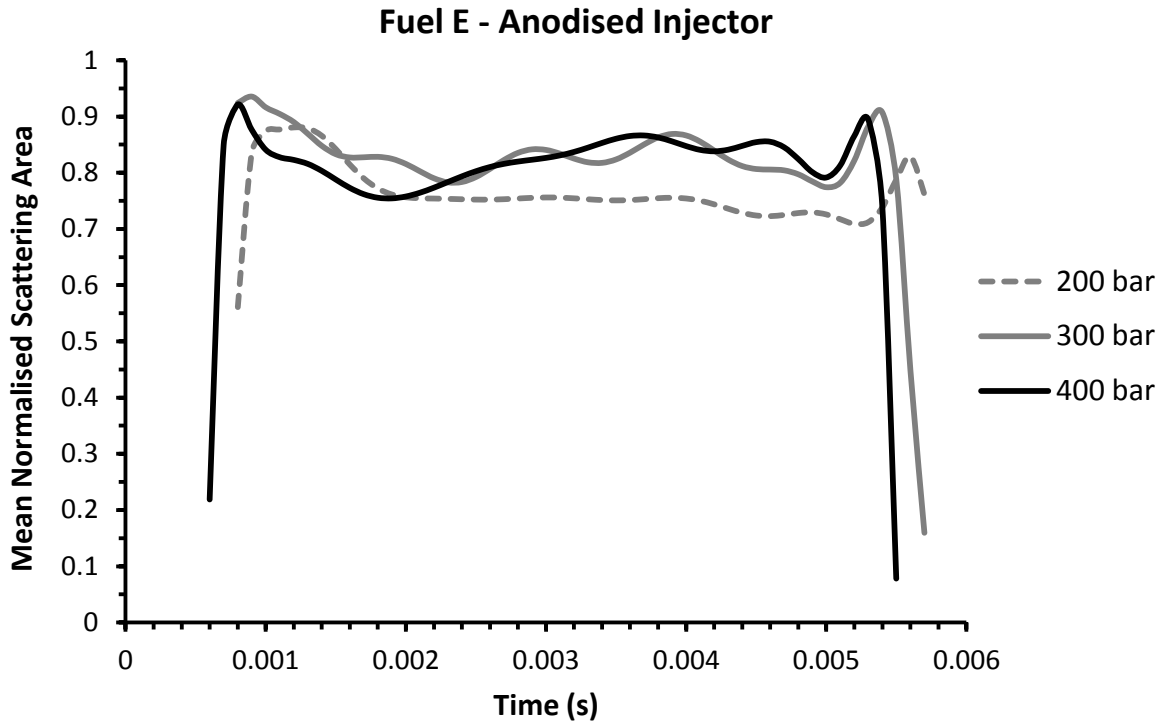


**Figure 11 (a): Graph of Normalised Cavitation Scattering Area for Fuel E as a Function of Time during the Injection for the Anodised Injector**

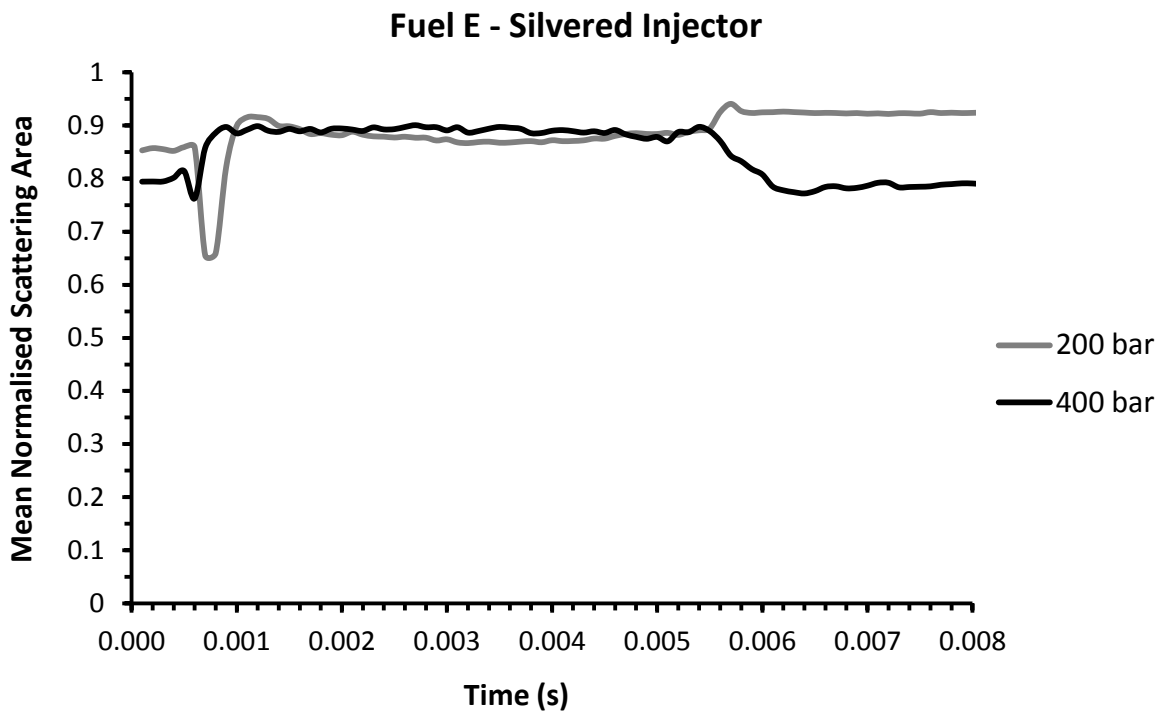


**Figure 11 (b): Graph of Normalised Cavitation Scattering Area for Fuel E as a Function of Time during the Injection for the Silvered Injector**

Two forms of internal cavitation flow are responsible for these observations. The first form of cavitation flow is geometric cavitation, which was formed at the entrance to the nozzle hole as a result of the low local pressure occurring near the entrance of the nozzle hole, immediately following the sharp edge defining the entrance to the hole. The fuel flow entering the hole began to cavitate as a result of the large acceleration and pressure gradient necessary to move the fluid from the annulus around the needle, past the sharply curved hole edges, and into the nozzle holes. A careful examination of the right hand image in Figure 5 and the image shown in Figure 6 shows the geometric cavitation occurring at the entrance to the nozzle holes. This form of cavitation contributed approximately 10 % to 15 % to the normalised cavitation scattering area at 400 bar common rail pressure.

The second form of cavitation flow developed as a result of vortex flow along the length of the nozzle holes. The flow vorticity in the holes resulted in a low pressure region near the central axis about which the fluid was rotating. If the low pressure region at the centre of the vortex flow had a local pressure lower than the saturated vapour pressure of the fluid, then the vortex flow may result in a vapour region developing near the central axis. This type of cavitation appears string-like within the fluid, and is referred to as string cavitation. The white foam-like structures observable in the nozzle passages in the right hand image in Figure 5, and the dark regions observable in the nozzle holes in Figure 6 show vortex generated string cavitation, which contributes approximately 85 % to 90 % to the normalised cavitation scattering area at 400 bar common rail pressure.

A second interesting feature is observable in Figures 7 to 11. As the common rail pressure was increased from 200 bar to 400 bar, the rising edge of the normalised cavitation scattering area was observed to occur earlier relative to the leading edge of the TTL injection pulse. This effect was caused by the common rail fuel pressure assisting the needle lift rate, facilitating a faster needle response. A corresponding effect occurred at the end of injection, when the decreasing common rail pressure resulted in a later needle return to the final closed position.

It should be noted from the (b) figures in Figures 7 to 11 that the normalised scattering areas appeared to be non-zero in the temporal regions outside of the injection time. This was observed as a significant non-zero signal because the diesel fuel formed fuel bubbles in the nozzle passages at the end of the fuel injection, which remained in the nozzle passages for

long time durations after the fuel injection was completed. These fuel bubbles were formed in the space below the needle and in the nozzle holes at the end of injection as a result of cavitation flow developing near the needle seal during the final stage of needle return (needle cavitation). These stationary fuel bubbles scattered incident white light away from the reflective silver surface of the silvered injectors, hence producing optical absorption signal which was then processed as described earlier in Section 4.

### 5.3 Cavitation Scattering Dependence on Fuel Properties

Figures 12 (a) and (b) show the mean normalised cavitation scattering area as a function of time during the injection for (a) the silvered injector, and (b) the anodised injector, respectively, for all five fuel samples, at 400 bar rail pressure. Figure 12(a) shows a clear ranking order for the five fuels. Fuel sample D produced the lowest mean normalised cavitation scattering area of the five tested fuel samples. This was followed by, in order of increasing normalised cavitation scattering area, sample E, sample C, sample A, and finally sample B, which produced the largest mean cavitation scattering area during the fuel injection.

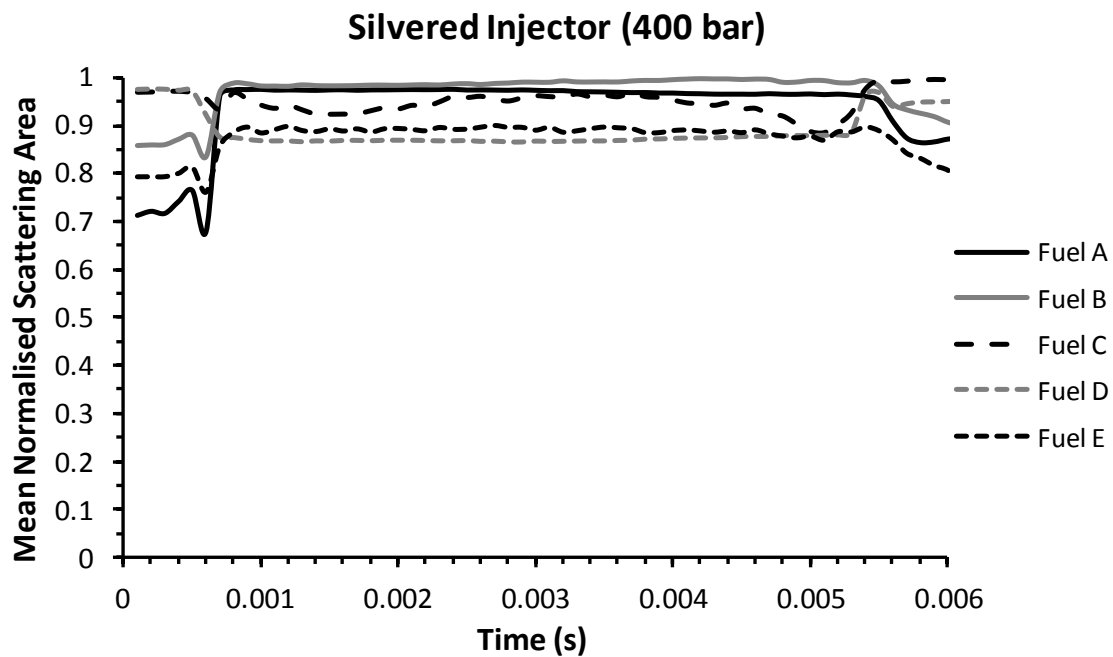


**Figure 12(a): Graph of Normalised Mean Cavitation Scattering Area Imaged as a Function of Time for the Five Fuel Samples (Silvered Injector).**

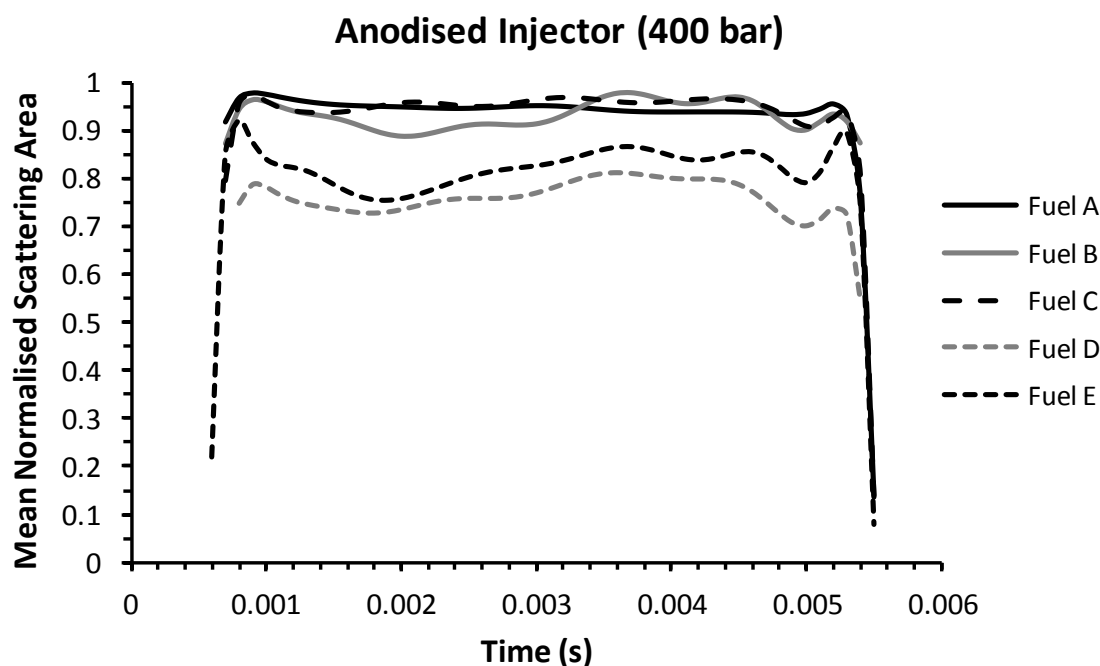


**Figure 12(b): Graph of Normalised Mean Cavitation Scattering Area Imaged as a Function of Time for the Five Fuel Samples (Anodised Injector).**

The graph presented in Figure 12 (b) shows that Fuel D produced the lowest normalised cavitation scattering area, followed by that obtained from sample E. These are consistent with the results shown in Figure 12 (a) for the silvered injector. Fuel samples A and C produced very similar normalised cavitation scattering area profiles as a function of time during the injection in the anodised injector. Sample B appeared to produce slightly smaller cavitation scattering area than samples A and C during needle lift, but this increased to be the largest during needle return. The large normalised cavitation scattering area obtained by fuel sample B in the later part of the fuel injection (observable in Figure 12 (b)) is consistent with the behaviour of sample B observable in Figure 12(a).

Consideration of the fuel properties presented in Tables 1 and 2, together with the graphs presented in Figure 12, leads to the conclusion that the fuel sample containing fatty acid methyl ester (FAME) (sample D) produced the lowest normalised cavitation scattering area during the injection. This may have been a consequence of the large boiling point temperature of the FAME additive, and the effect it had on the distillation profile of the fuel sample.

Indeed, it appears that the addition of FAME to sample A has had a greater effect on the normalised cavitation scattering area, injected mass and discharge coefficient that would have been suggested by consideration of its effect on the distillation profile only. A comparison of the distillation profiles of diesel sample C and D reveals that sample C had a distillation profile relative to D that was shifted to larger temperatures by approximately 25 °C per 10 % distillation interval. However, fuel injection with sample D produced a significantly larger injected mass and discharge coefficient, and correspondingly lower normalised cavitation scattering area than sample C.

These results also appear to confirm the suggestion of Li [30] and Postrioti *et al* [31] that biodiesel has a propensity to produce less internal cavitation than conventional diesel. They suggested this during their investigation into the relative properties of fuel jets obtained from conventional diesel and biodiesel fuels.

The simultaneous effect of viscosity and distillation profile on cavitation may be established by consideration of the mean normalised cavitation scattering area profiles of samples B and C in Figures 12 (a) and (b). In Figure 12 (a), it is clear that sample B produces a larger cavitation scattering area profile than sample C over the entire injection period. In Figure 12 (b), sample B produces a lower cavitation scattering area than sample C during needle lift, which then increases to a larger scattering area during needle return. This suggests that as fuel viscosity increases and distillation profile shifts to larger temperatures, the cavitation volume in the nozzles decreases (as indicated by a decrease in the normalised cavitation scattering area), resulting in an expected increase in the mean discharge coefficient.

Support for this argument is supplied by a consideration of the flow properties associated with fuel samples B and C, presented in Table 2. Sample C has a 95 % larger kinematic viscosity than sample B, together with a distillation profile shifted to larger temperatures. This has the consequence that sample C produces a mean volume flow rate and discharge coefficient that is 1.1 % larger than that produced by sample B.

Fuels with larger relative viscosity and the same boiling profile will produce a lower rate of strain than fuels with lower relative viscosity when entering or flowing through a tube. The relationship between the local strain rate and the local pressure gradient during flow acceleration would suggest that a fuel with a small relative viscosity would exhibit a

propensity to cavitate earlier than a fuel with a large relative viscosity. It might also suggest that a fuel with small relative viscosity will produce a larger cavitation volume than a fuel with relatively large viscosity.

#### **5.4 Cavitation Scattering, Injected Fuel Mass and Nozzle Discharge Coefficient**

The total injected fuel mass from a conventional VCO injector operating at 400 bar rail pressure was obtained from all of the fuel samples, for 1,000 successive injections. The mean injected fuel mass per injection for each fuel sample was obtained by dividing the total injected fuel mass by 1,000. These results are presented in Table 2.

The temporal mean value of the normalised cavitation scattering area was obtained for each fuel sample at 400 bar rail pressure, for both the silvered injector and the anodised injector, by finding the mean value of the normalised mean cavitation scattering area obtained during the injection.

The graphs of the temporal mean normalised cavitation scattering area obtained from Figure 12 (a) and (b) were plotted against mean injected fuel mass for all of the fuels. These data are presented in Figure 13 (a) and (b) respectively, together with a best fit straight line. Figures 13 (a) and (b) show that the temporal mean normalised cavitation scattering area for the five fuels lie close to the best fit straight line curve inserted into the graph.

Figures 13 (a) and (b) show that the injected fuel mass increased as the normalised cavitation scattering area decreased. This would suggest that the cavitation flow occurring inside the injector nozzles served to choke the fuel flow through the nozzles, reducing the injected fuel mass. This suggests that the vapour pockets occurring in the nozzles as a result of the cavitation, affects the discharge coefficient negatively by taking up necessary volume which should be occupied by flowing liquid fuel.

This is explored further in Figures 14 (a) and (b), which present graphs of the mean discharge coefficient for each fuel sample (taken from Table 2), plotted against the temporal mean normalised scattering area. Figures 14 (a) and (b) show that the discharge coefficient decreases for the different fuel samples, as the mean normalised scattering areas increase. This supports the previous suggestion that the vapour volume occupying the nozzles acts as a

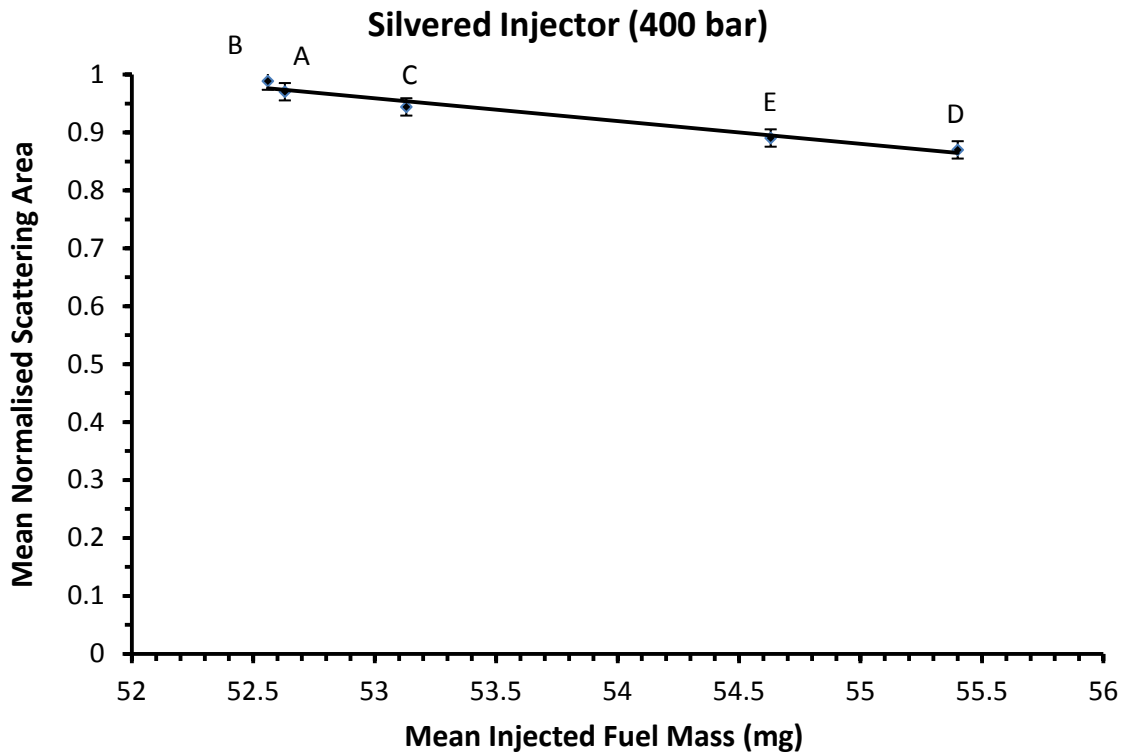


**Figure 13(a): Graph of Normalised Mean Cavitation Scattering Area Imaged as a Function of Mean Injected Fuel Mass for the Five Fuel Samples (Silvered Injector).**

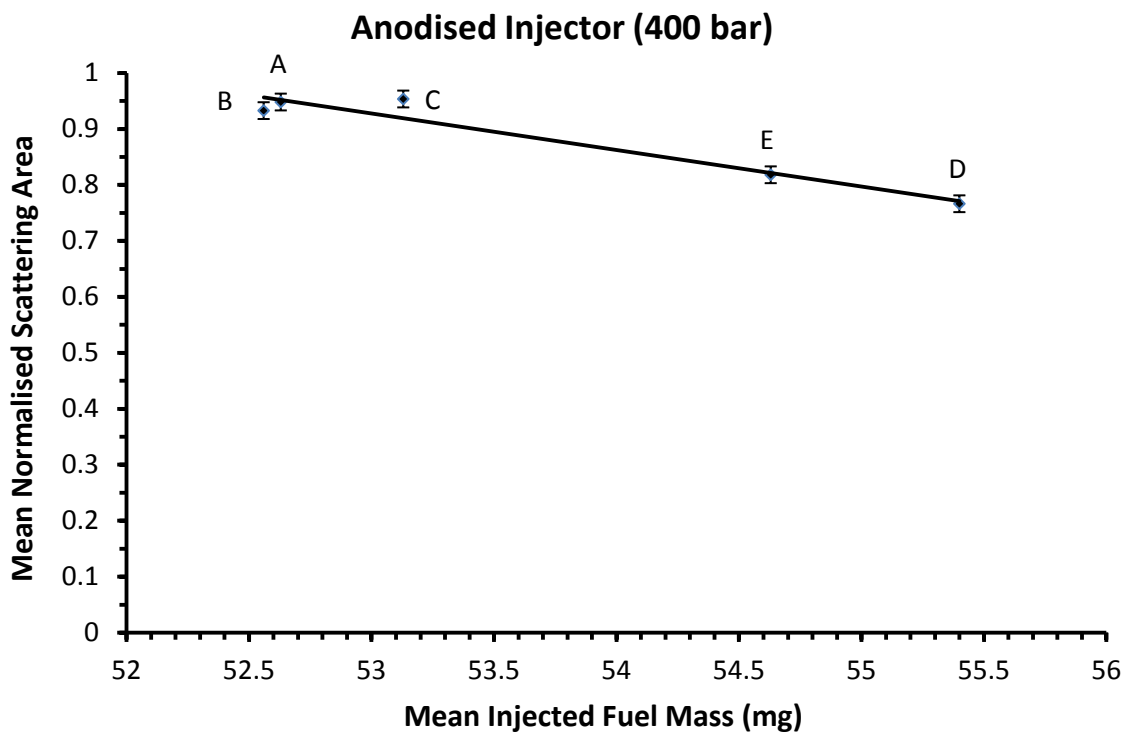


**Figure 13(b): Graph of Normalised Mean Cavitation Scattering Area Imaged as a Function of Mean Injected Fuel Mass for the Five Fuel Samples (Anodised Injector).**

choke, reducing the mass of injected diesel fuel. However, in Figure 14 (b), the mean normalised scattering area for sample B appears to be smaller than for samples A and C. This is a consequence of the unusual time-dependent cavitation scattering area profile shown in Figure 12 (b). It should be noted from Figure 12 (b) that during needle return, sample B produced a larger cavitation scattering area than samples A and C, consistent with what is graphically presented in Figures 12 (a), 13 (a), and 14(a).

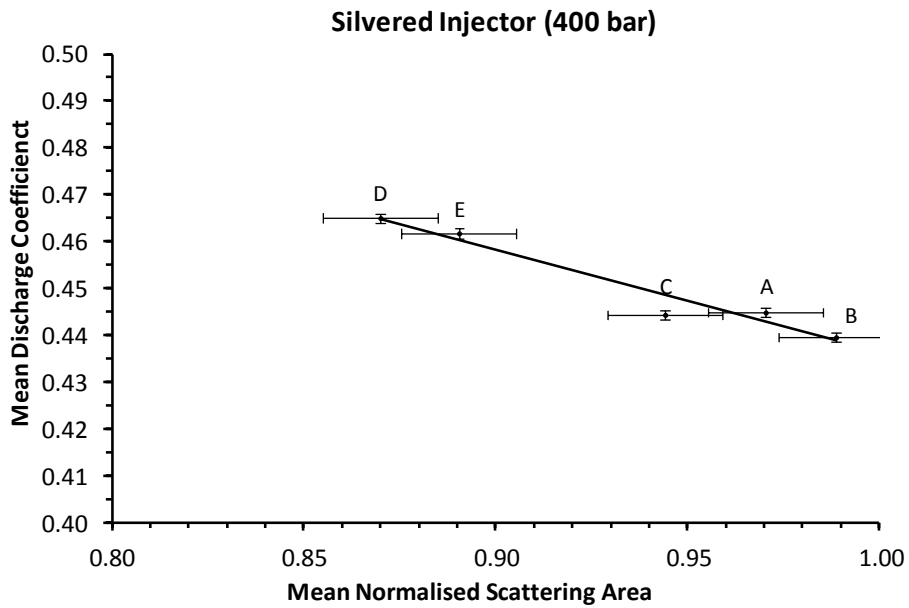


**Figure 14(a): Graph of Discharge Coefficient as a Function of Mean Normalised Cavitation Scattering Area for the Five Fuel Samples (Silvered Injector).**

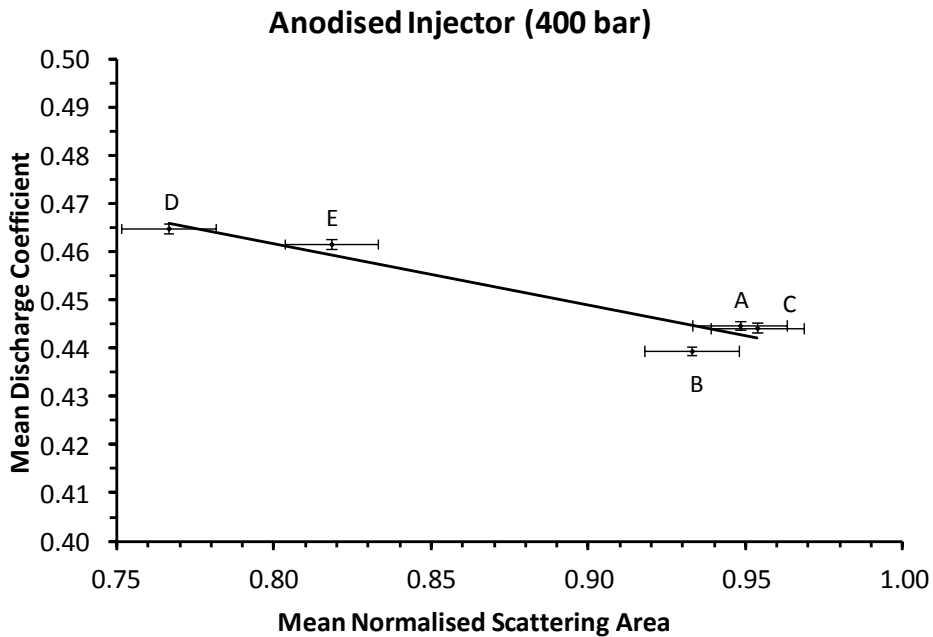


**Figure 14(b): Graph of Discharge Coefficient as a Function of Mean Normalised Cavitation Scattering Area for the Five Fuel Samples (Anodised Injector).**

## 6. CONCLUSION

A novel optical method for the assessment of diesel nozzle flow has been developed in order to discriminate between the cavitation volume occupied by different diesel fuels during the fuel injection process. The method is based on high resolution, fast video photography of elastic scattering of white light from the surface defining the liquid-vapour interface formed during nozzle cavitation flow. The time-resolved scattering data was converted to the proportion of nozzle area producing cavitation scattering, which was termed the normalised cavitation scattering area. The expectation was that the normalised cavitation area would be indirectly linked to the volume of vapour forming in the nozzles during the cavitation process.

A number of durability and consistency tests were performed prior to the execution of the experiment. The time-resolved normalised cavitation area was obtained from three identical injector tips at 300 bar and 400 bar rail pressure. They were observed to vary from the mean by approximately 1.5 %. This set a limit on the variability of the cavitation area as a function of any manufacturing variations.

The following specific conclusions can be drawn from this experiment:

1. Geometric and string cavitation were observed in the diesel nozzles during diesel fuel injection. The geometric cavitation and the string cavitation contributed approximately 10 % to 15 %, and 85 % to 90 %, to the total imaged cavitation area respectively, at 400 bar rail pressure.
2. The normalised cavitation scattering area was observed to increase as a function of increased rail pressure over the pressure range 200 bar - 400 bar. This applied to all of the diesel fuels tested, and to both injectors. This suggests that the volume of vapour occupying the nozzle passages increased with an increase in common rail pressure.
3. A ranking order of the normalised cavitation scattering areas for the five fuels tested was observed. Diesel fuel sample D was observed to produce the smallest cavitation area, followed by, in increasing order, fuel samples E, C, A and B respectively. Fuel samples D and E contained 20 % fatty acid methyl ester (FAME) additive v/v, and a proprietary additive

respectively, which accounted for the low cavitation scattering areas observed, and the relatively large injected fuel masses, mean nozzle velocities and mean discharge coefficients.

The addition of 25% FAME v/v to sample A to form B20 bio-diesel sample D appeared to produce a more significant effect on the injected mass, discharge coefficient, and reduction in cavitation vapour volume than is suggested by consideration of the viscosity and distillation profile only.

4. An inverse relationship between the mean cavitation scattering areas obtained from the fuel samples and the corresponding mean injected fuel masses was discovered. This suggested that the mean injected fuel mass decreased as the volume of fuel vapour in the nozzle holes increased. This conclusion was supported further by the inverse relationship that was shown to exist between the mean discharge coefficients and the mean normalised cavitation scattering areas obtained from the five fuel samples.

5. An increase in kinematic viscosity, together with a temperature-shifted distillation profile (sample C relative to B), resulted in a decrease in cavitation vapour volume occupying the nozzle passages. This resulted in a corresponding increase in injected fuel mass and discharge coefficient.

Finally, an alternative approach to that reported here may be achieved by altering the camera viewing perspective. The camera captured bottom-view images of the flow in the region below the needle, and in the nozzle holes. The camera orientation in the experiments reported here resulted in high speed imaging of back-scattered light and optical absorption in the anodised and silvered injectors respectively.

Changing the camera view in order to image cavitation flow scattering at 90 deg to the incident white light should offer the viewer the opportunity to observe the cavitation flow from the side, and resolve different forms of cavitation flow explicitly (geometric cavitation, string cavitation etc).

## **ACKNOWLEDGEMENTS**

The authors would like to acknowledge Shell Global Solutions for partial support for this work. In addition, the authors would like to acknowledge the contributions of Professor C. Arcoumanis to the research project, and the valuable assistance of School of Engineering technical staff, particularly Mr J. Ford, Mr T. Fleming, Mr M. Smith and Mr J. Kenny.

## REFERENCES

1. H. Chaves, M. Knapp, A. Kubitzek, and F. Obermeier, *Experimental Study of Cavitation in the Nozzle Hole of Diesel Injectors Using Transparent Nozzles*. SAE Paper 950290, 1995.
2. C. Badock, R. Wirth, A. Fath, and A. Leipertz, *Investigation of cavitation in real size diesel injection nozzles*. International Journal of Heat and Fluid Flow, 20(5), pp. 538-544, 1999.
3. A. Andriotis, M. Gavaises, C. Arcoumanis, *Vortex flow and cavitation in diesel injector nozzles*, Journal of Fluid Mechanics, vol 610, pp. 195 - 215, 2008.
4. C. Arcoumanis and M. Gavaises, *Cavitation in diesel injectors: modelling and experiments*. Proceedings of the 14th ILASS-Europe Annual Conference, Manchester, England, 1998.
5. J.H. Kim, K. Nishida, H. Hiroyasu, *Characteristics of the Internal Flow in a Diesel Injection Nozzle*. ICLASS-97, 1997.
6. C. Soteriou, R. Andrews, M. Smith, *Direct Injection Diesel Sprays and the Effect of Cavitation and Hydraulic Flip on Atomization*, SAE paper, 1995 (950080).
7. C. Soteriou, M. Smith, R.J. Andrews, *Cavitation Hydraulic Flip and Atomization in Direct Injection Diesel Sprays*. IMechE Paper C465/051/93, 1993.
8. C. Arcoumanis, M. Gavaises, J.M. Nouri, E. Abdul-Wahab, *Analysis of the flow in the nozzle of a vertical multi-hole diesel engine injector*, . SAE paper, 1998 (980811).
9. C. Soteriou, R. Andrews, M. Smith, N. Torres, S. Sankhalpara, *The Flow Patterns and Sprays of Variable Orifice Nozzle Geometries for Diesel Injection*. SAE paper, 2000 (2000-01-0943).
10. J.M. Desantes, R. Payri, F.J. Salvador, J. Gimeno, *Measurements of Spray Momentum for the Study of Cavitation in Diesel Injection Nozzles*. SAE paper, 2003 (2003-01-0703).

11. F. Payri, V. Bermudez, R. Payri, F.J. Salvador, *The influence of cavitation on the internal flow and the spray characteristics in diesel injection nozzles*. Fuel. Vol. 83. 2004, 419 - 431.
12. K. Nishida, S. Ceccio, D. Assanis, N. Tamaki, H. Hiroyasu, *Characterization of Cavitation Flow in a Simple Hole Nozzle*. ICLASS-97, 1997.
13. C. Soteriou, M. Smith, R. Andrews, *Diesel injection: laser light sheet illumination of the development of cavitation in orifices*. IMechE Conference Transactions, 1998 (C529/018/98).
14. A. Osman, *Failure of a diesel engine injector nozzle by cavitation damage*, Engineering Failure Analysis vol. 13 issue 7, October 2006, 1126 – 1133.
15. N. Tait, Shell Global Solutions, Personal Communication, 2008.
16. C. Badock, R. Wirth, and C. Tropea. *The Influence of Hydro Grinding on Cavitation inside a Diesel Injection Nozzle and Primary Break-Up under Unsteady Pressure Conditions*. in *Proc. ICLASS-EUROPE*. Toulouse, France. 1999.
17. L. He and F. Ruiz, *Effect of cavitation on flow and turbulence in plain orifices for high-speed atomization*. Atomization and Sprays, **5**(6) (1995) 569 - 584.
18. M.E. Henry and S.H. Collicott, *Visualization of internal flow in a cavitating slot orifice*. Atomization and Sprays, **10**(6): pp. 545-563, 2000.
19. H. Roth, M. Gavaises, C. Arcoumanis, *Cavitation Initiation, its Development and Link with Flow Turbulence in Diesel Injector Nozzles*. SAE paper, 2002 (2002-01-0214).
20. H. Roth, *Experimental and Computational Investigation of Cavitation in Diesel Injector Nozzles*. PhD Thesis, Imperial College, 2004.
21. N. Mitroglou, *Multi-hole Injectors for Direct-Injection Gasoline Engines*, PhD Thesis, City University London, 2005.

22. M. Gavaises and A. Andriotis, *Cavitation Inside Multi-hole Injectors for Large Diesel Engines and its Effects on the Near-nozzle Spray Structure*. SAE paper, 2006 (2006-01-1114).
23. J.M. Nouri, N. Mitroglou, N. Yan, C. Arcoumanis, *Internal flow and cavitation in a multi-hole injector for gasoline direct injection engines*. SAE paper, 2007 (2007-01-1405).
24. A. Andriotis, M. Spathopoulou, M. Gavaises, *Effect of Nozzle Flow and Cavitation Structures on Spray Development in Low-speed Two-Stroke Diesel Engines*. International Council on Combustion Engines, CIMAC Congress, Vienna, 2007 (Paper 262).
25. C. Arcoumanis, M. Badami, H. Flora, M. Gavaises, *Cavitation in Real-Size, Multi-Hole Diesel Injector Nozzles*, SAE Transactions Journal of Engines, 2000-01-1249, 109-3, 2000.
26. C. Arcoumanis, M. Gavaises, H. Flora, H. Roth, *Visualisation of cavitation in diesel engine injectors*. *Mecanique & Industries*, 2001(5).
27. M. Blessing, G. Konig, C. Kruger, U. Michels, and V. Schwarz, *Analysis of Flow and Cavitation Phenomena in Diesel Injection Nozzles and its Effects on Spray and Mixture Formation*. SAE paper, 2003 (2003-01-1358).
28. R. Miranda, H. Chaves, U. Martin, F. Obermeier, *Cavitation in Transparent Real Size VCO Injection Nozzle*, Paper 12-6, Proceedings of ICLASS 2003, Sorrento, Italy, 2003.
29. H. Roth, E. Giannadakis, M. Gavaises, C. Arcoumanis, K. Omae, I. Sakata, M. Nakamura, and H. Yanagihara, *Effect of Multi-Injection Strategy on Cavitation Development in Diesel Injector Nozzle Holes*. SAE paper, 2005 (2005-01-1237).
30. L. Li, *Experimental Study of Biodiesel Spray and Combustion Characteristics*. SAE paper, 2006 (2006-01-3250).
31. L. Postrioti, C.N. Grimaldi, M. Ceccobello, and R. DiGioia, *Diesel Common Rail Injection System Behaviour with Different Fuels*. SAE paper, 2004 (2004-01-0029).

32. R.D. Lockett, L. Liverani, D. Thaker, C. Arcoumanis, *The characterisation of diesel cavitating flow using time-resolved light scattering*, Conference on Injection Systems for IC Engines, C677/020/09, pp 163 - 171, IMechE, 2009.

33. L.A. Dombrovsky, S.S. Sazhin, S.V. Mikhalovsky, R. Wood, and M.R. Heikal, *Spectral properties of diesel fuel droplets*, Fuel 82 (2003) 15 - 22.